

## Structure and Electrochemical Performance of $\text{Li}[\text{Li}_{0.2}\text{Co}_{0.4}\text{Mn}_{0.4}]\text{O}_2$ Cathode Material for Lithium Ion Battery by Co-precipitation Method

X. Wei, X. X. Lu, S. C. Zhang\*, G. R. Liu

*School of Materials Science and Engineering, Beihang University, Beijing 100191, PR China*

(Received 09 June 2013; published online 02 September 2013)

The nano-structured  $\text{Li}[\text{Li}_{0.2}\text{Co}_{0.4}\text{Mn}_{0.4}]\text{O}_2$  cathode material is synthesized by a co-precipitation method. X-ray diffraction shows that the synthesized material has a hexagonal  $\alpha\text{-NaFeO}_2$  type structure with a space group  $R\bar{3}m$ . Scanning electron microscopy and transmission electron microscopy images show the homogeneous distribution with 100-200 nm. X-ray photoelectron spectroscopy results indicate that the oxidation states of Co and Mn in  $\text{Li}[\text{Li}_{0.2}\text{Co}_{0.4}\text{Mn}_{0.4}]\text{O}_2$  are present in trivalence and tetravalence, respectively. The charge-discharge curves and cycling performance are analyzed in detail. The initial charge and discharge capacities are respectively 236.5 mAh  $\text{g}^{-1}$  and 140.3 mAh  $\text{g}^{-1}$  at the current density of 100 mA  $\text{g}^{-1}$  in the voltage range of 2.0-4.6 V.

**Keywords:** Li-ion battery;  $\text{Li}[\text{Li}_{0.2}\text{Co}_{0.4}\text{Mn}_{0.4}]\text{O}_2$ ; Co-precipitation Method; Li-rich layered material; Cathode.

PACS numbers: 81.07.-b, 82.47.Jk

### 1. INTRODUCTION

Lithium ion batteries were considered to be a promising electric storage technology for electric vehicles. A vast series of Li-storage cathode materials had been explored in the past two decades.  $\text{LiCoO}_2$  had been widely applied due to its good electrochemical performance and its ease of preparation. However, the concerns about high costs, toxicity and structural instability prompted a search for alternative cathode materials. Manganese substitution was considered because it was more abundant and cheaper than Cobalt. Li-rich cathode materials  $x\text{LiCoO}_2 \cdot (1-x)\text{Li}_2\text{MnO}_3$  have been studied in the recent past [1-3]. In these materials,  $\text{Li}_2\text{MnO}_3$  existed with short-range order within a  $\text{LiCoO}_2$  matrix [4].  $\text{Li}^+$  extraction and oxygen loss from lattice were concurrent at the first charge process of Li-rich layered materials. A part of  $\text{Mn}^{4+}$  ions was activated to participate in the following electrochemical reactions, leading to a high discharge capacity [5]. Among the different stoichiometric ratio of  $x\text{LiCoO}_2 \cdot (1-x)\text{Li}_2\text{MnO}_3$  compounds,  $\text{Li}[\text{Li}_{0.2}\text{Co}_{0.4}\text{Mn}_{0.4}]\text{O}_2$  have been studied by many authors. To improve the performance of  $\text{Li}[\text{Li}_{0.2}\text{Co}_{0.4}\text{Mn}_{0.4}]\text{O}_2$  materials, some groups have recently adopted different synthetic methods, such as sol-gel method [6], solid state method [7, 8], oxalate-precursor method [9].

In this work, we developed a simple co-precipitation method to synthesize nano-structured  $\text{Li}[\text{Li}_{0.2}\text{Co}_{0.4}\text{Mn}_{0.4}]\text{O}_2$  particles. The structure, morphology and electrochemical properties were thoroughly investigated.

### 2. EXPERIMENTAL

The  $\text{Li}[\text{Li}_{0.2}\text{Co}_{0.4}\text{Mn}_{0.4}]\text{O}_2$  sample was synthesized by a co-precipitation method. The procedure was described as follows. The desired amount of  $\text{Co}(\text{NO}_3)_2 \cdot 6\text{H}_2\text{O}$ ,  $\text{MnCl}_2 \cdot 4\text{H}_2\text{O}$  were dissolved to form a aqueous solution.  $\text{M}(\text{OH})_2$  ( $\text{M} = \text{Co}, \text{Mn}$ ) precipitate was gained by slowly dripping the above solution and  $\text{LiOH}$  solution synchronously into a glass reactor with

continuous string. The pH value of the reactant solution was adjusted by ammonia and was kept at 11. The hydroxide precipitate was filtrated, washed and dried. The mixture of precipitate and  $\text{LiOH} \cdot \text{H}_2\text{O}$  were ground and initially heat-treated at 500 °C for 5 h for the impregnation of Lithium into the matrix. The final product was finally obtained by sintering at 800 °C for 10 h and then quenching to room temperature.

X-ray diffraction (XRD, Rigaku D/Max-2400, Japan) using Cu K $\alpha$  radiation was used to identify the crystalline structure of the synthesized materials. Scanning electron microscopy (SEM, Hitachi S-4800, Japan), transmission electron microscopy (TEM, JEM-2100F, Japan) were engaged to observe morphology, size and distribution of as-prepared material. X-ray photoelectron spectroscopy (XPS) was obtained by using ESCALAB250 (Thermo Fisher Scientific) with monochromatic Al K $\alpha$  anode source with pass energy of 20 eV and energy step of 0.1 eV. The chemical valence state of the transition metal elements was determined.

The electrode slurry was prepared by mixing 80 wt.% active material, 10 wt.% carbon black, and 10 wt.% polyvinylidene fluoride (PVDF) with *n*-methyl-2-pyrrolidone (NMP). The prepared slurry was pasted onto an aluminum foil. The electrode was then dried in a vacuum oven at 100 °C for 2 h. The testing half-cells were assembled in an argon-filled glove box (MB-10-G with TP170b/mono, MBRAUN) with lithium metal as counter and reference electrode. Electrolyte was 1 M  $\text{LiPF}_6$  in a mixed solution of EC and DMC (1:1 in volume ratio). The charge-discharge measurements were galvanostatically carried out by using a battery test system (NWEARE BTS-610, Neware Technology Co., Ltd., China). All the batteries were tested over a voltage range between 2.0 V and 4.6 V *vs.*  $\text{Li}^0/\text{Li}^+$  at room temperature.

### 3. RESULTS AND DISCUSSION

\* csc@buaa.edu.cn

Fig. 1 shows the X-ray diffraction pattern of  $\text{Li}[\text{Li}_{0.2}\text{Co}_{0.4}\text{Mn}_{0.4}]\text{O}_2$  sample. All the major diffraction peaks can be indexed as a layered oxide lattice based on a hexagonal  $\alpha\text{-NaFeO}_2$  type structure with a space group  $R\bar{3}m$  [10]. The weak peaks between  $21^\circ$  and  $25^\circ$  are reflected by a monoclinic unit cell with a  $C2/m$  symmetry, due to a  $\text{LiMn}_6$  cation arrangement that occurs in the transition metal layers of  $\text{Li}_2\text{MnO}_3$  regions [11]. Both (006)/(102) and (108)/(110) doublets are clear split, suggesting that the material crystallized in the layered structure without formation of any spinel structure [11].

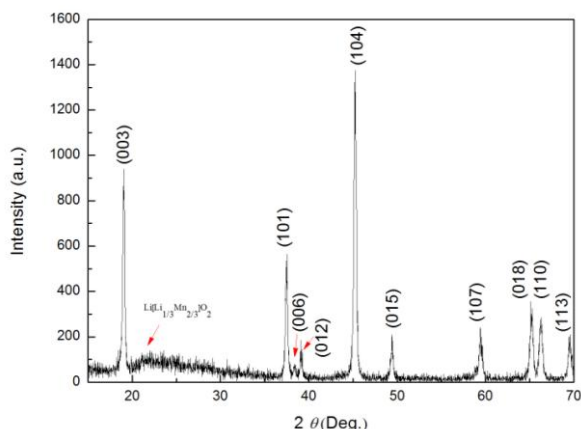


Fig. 1 – X-ray diffraction pattern of  $\text{Li}[\text{Li}_{0.2}\text{Co}_{0.4}\text{Mn}_{0.4}]\text{O}_2$  sample

Fig. 2 shows the SEM and TEM images of  $\text{Li}[\text{Li}_{0.2}\text{Co}_{0.4}\text{Mn}_{0.4}]\text{O}_2$  sample. It can be observed that homogeneous particles with dimensions in a narrow range between 100 nm and 200 nm. Undoubtedly, such nano-sized particles must result in a high surface area and a short diffusion path for Li insertion/extraction and also for the diffusive transport of the oxygen ion vacancies, so as to enhance the electrochemical performance, especially the high rate capacity [12].

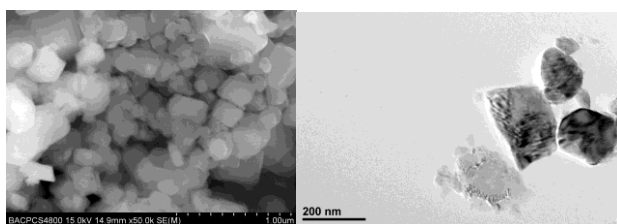


Fig. 2 – SEM and TEM images of  $\text{Li}[\text{Li}_{0.2}\text{Co}_{0.4}\text{Mn}_{0.4}]\text{O}_2$  sample.

Fig. 3 shows  $\text{Co}2p$  and  $\text{Mn}2p$  XPS spectra of as-prepared material. The chemical valence state of the transition metal elements is determined. In Fig. 3A, the results show a  $\text{Co}2p_{3/2}$  main peak at 780.9 eV with a satellite peak at 790.3 eV and a  $\text{Co}2p_{1/2}$  main peak at 795.9 eV with a satellite peak at 805.2 eV. It confirms that the main oxidation state is  $\text{Co}^{3+}$  [13, 14]. In the  $\text{Mn}2p$  spectra (Fig. 3B), the major peak  $\text{Mn}2p_{3/2}$  at 643.1 eV confirms the  $\text{Mn}^{4+}$  oxidation states in this material, in accord with previous reports [15, 16].

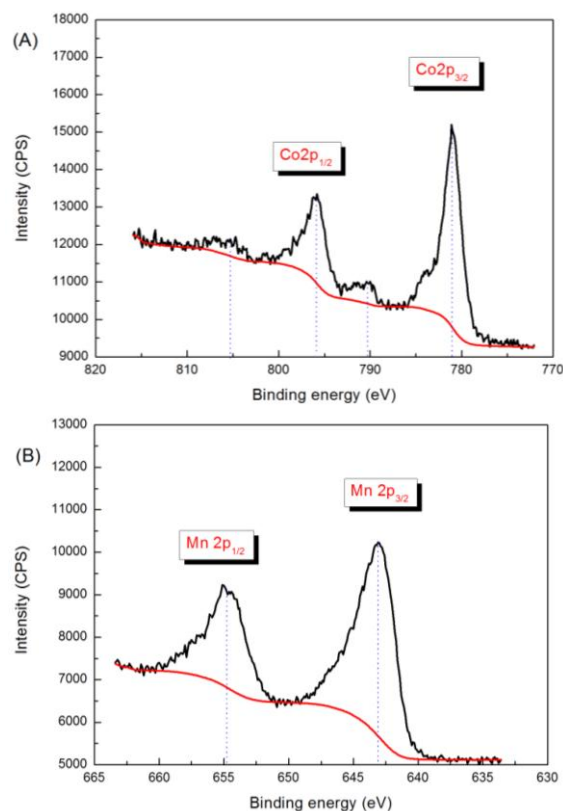
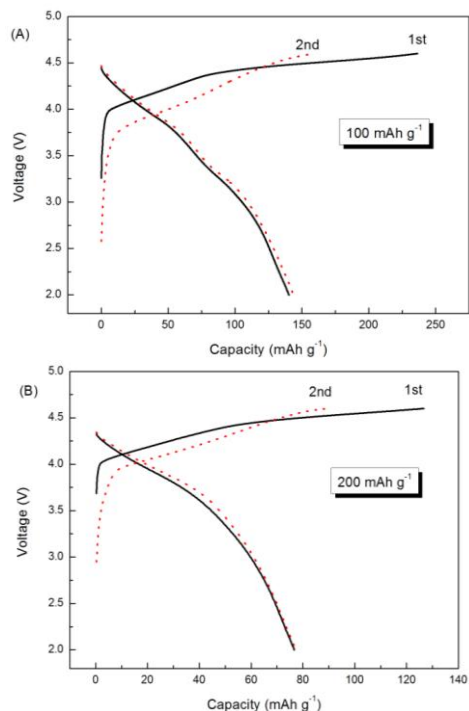


Fig. 3 –  $\text{Co}2p$  (A) and  $\text{Mn}2p$  (B) XPS spectra of  $\text{Li}[\text{Li}_{0.2}\text{Co}_{0.4}\text{Mn}_{0.4}]\text{O}_2$  sample

Fig. 4 shows the 1st (A) and 2nd (B) cycles charge-discharge curves for  $\text{Li}[\text{Li}_{0.2}\text{Co}_{0.4}\text{Mn}_{0.4}]\text{O}_2$  sample between 2.0 and 4.6 V at the current density of 100 and 200  $\text{mA g}^{-1}$ . In the first charge process, the slope of 4.0–4.4 V corresponds to the oxidation of the transition metal ( $\text{Co}^{3+} \rightarrow \text{Co}^{3.6}$ ) [1], and a long plateau at  $\sim 4.5$  V corresponds to oxygen loss with Li extraction, attributing to active process of  $\text{Li}_2\text{MnO}_3$  ( $\text{Li}_2\text{MnO}_3 \rightarrow 2\text{Li}^+ + 2e^- + 0.5\text{O}_2 + \text{MnO}_2$ ) [17]. The long plateau vanishes during the subsequent charge cycles. After this irreversible structural transformation, both  $\text{Co}^{3.6+}$  and  $\text{Mn}^{4+}$  can be reduced in the first discharge process. The sample delivers the first charge capacity of 236.5  $\text{mAh g}^{-1}$  and the first discharge capacity of 140.3  $\text{mAh g}^{-1}$  at the current density of 100  $\text{mA g}^{-1}$ , with the coulombic efficiency of 59.3%. The sample delivers the first charge capacity of 126.5  $\text{mAh g}^{-1}$  and the first discharge capacity of 76.6  $\text{mAh g}^{-1}$  at the current density of 200  $\text{mA g}^{-1}$ , with the coulombic efficiency of 60.5%. The 2nd charge capacities are respectively 158.2 and 88.8  $\text{mAh g}^{-1}$  and discharge capacities are respectively 143.8 and 77.3  $\text{mAh g}^{-1}$ , corresponding to the current density of 100 and 200  $\text{mA g}^{-1}$ , respectively, with the coulombic efficiency of 90.9% and 87.0%. After 100th cycles (Fig. 5), the retained discharge capacities are respectively 119.1 and 95.9  $\text{mAh g}^{-1}$ , which are 83.2%, and 124.1% of their 2nd discharge capacities, corresponding to the current density of 100 and 200  $\text{mA g}^{-1}$ . The cycling process accompanies with activation process of  $\text{Li}_2\text{MnO}_3$  component and capacity decay. Activation process undergoes a longer duration with higher current density. It can be observed that the discharge capacity ascends in the beginning several cycles and then descends in the sub-

sequent cycles from two profiles. The activation process of  $\text{Li}_2\text{MnO}_3$  component plays a main role in the ascending part. The descending part may be ascribed to the irreversible capacity loss caused by structural collapse during intercalation/deintercalation of  $\text{Li}^+$ . The degree of decline enlarges at lower current density, probably due to the more serious structure damage during the deeper charge and discharge process.



**Fig. 4** – The 1st (A) and 2nd (B) cycles charge-discharge curves of  $\text{Li}[\text{Li}_{0.2}\text{Co}_{0.4}\text{Mn}_{0.4}]\text{O}_2$  sample at the current density of 100 and  $200 \text{ mA g}^{-1}$ .

## REFERENCES

1. T. A. Arinkumar, Y. Wu and A. Manthiram, *Chem. Mater.* **19**, 3067 (2007).
2. Y. Wu and A. Manthiram, *Solid. State. Ionics* **180**, 50 (2009).
3. G. Singh, W. C. West, J. Soler and R. S. Katiyar, *J. Power Sources* **218**, 34 (2012).
4. S. H. Kang, C. S. Johnson, J. T. Vaughey, K. Amine and M. M. Thackeray, *J. Electrochem. Soc.* **153**, A1186 (2006).
5. M. M. Thackeray, S. H. Kang, C. S. Johnson, J. T. Vaughey, R. Benedek and S. A. Hackney, *J. Mater. Chem.* **17**, 3112 (2007).
6. Z. Li, Y. Wang, X. Bie, K. Zhu, C. Wang, G. Chen and Y. Wei, *Electrochem. Commun.* **13**, 1016 (2011).
7. J. Barenó, M. Balasubramanian, S. H. Kang, J. G. Wen, C. H. Lei, S. V. Pol, I. Petrov and D. P. Abraham, *Chem. Mater.* **23**, 2039 (2011).
8. J. G. Wen, J. Barenó, C. H. Lei, S. H. Kang, M. Balasubramanian, I. Petrov and D. P. Abraham, *Solid. State. Ionics* **182**, 98 (2011).

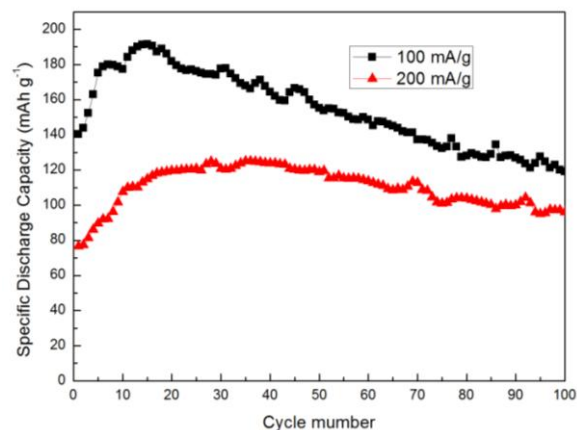


**Fig. 5** – Galvanostatic cycling performance of  $\text{Li}[\text{Li}_{0.2}\text{Co}_{0.4}\text{Mn}_{0.4}]\text{O}_2$  sample for 100 cycles.

## 4. CONCLUSIONS

The nano-sized material  $\text{Li}[\text{Li}_{0.2}\text{Co}_{0.4}\text{Mn}_{0.4}]\text{O}_2$  was synthesized by a co-precipitation method. After 100th cycles, the retained discharge capacities are respectively 119.1 and  $95.9 \text{ mAh g}^{-1}$ , which are 83.2%, and 124.1% of their 2nd discharge capacities, corresponding to the current density of 100 and  $200 \text{ mA g}^{-1}$ . Much work needs to be done in order to meet its commercial application.

## ACKNOWLEDGEMENTS

This work was supported by the National Basic Research Program of China (973 Program) (2013CB934001), National Natural Science Foundation of China (51074011 and 51274017) and National 863 Program (2007AA03Z231 and 2011AA11A257).

9. D. Luo, G. S. Li, X. F. Guan, C. Yu, J. Zheng, X. H. Zhang and L. P. Li, *J. Mater. Chem. A* **1**, 1220 (2013).
10. J. Gao and A. Manthiram, *J. Power Sources* **191**, 644 (2009).
11. Z. H. Lu, L. Y. Beaulieu, R. A. Donabarger, C. L. Thomas and J. R. Dahn, *J. Electrochem. Soc.* **149**, A778 (2002).
12. B. H. Song, Z. W. Liu, M. O. Lai and L. Lu, *Phys. Chem. Chem. Phys.* **14**, 12875 (2012).
13. J. Zheng, S. N. Deng, Z. C. Shi, H. J. Xu, H. Xu, Y. F. Deng, Z. Zhang and G. H. Chen, *J. Power Sources* **221**, 108 (2013).
14. K. J. K. Beng Jit Tan, Peter M. A. Sherwood, *J. Am. Chem. Soc.*, **113**, 855 (1991).
15. C. J. Jafta, K. I. Ozoemena, M. K. Mathe and W. D. Roos, *Electrochim. Acta* **85**, 411 (2012).
16. J. S. Park, K. C. Roh, J. W. Lee, K. Song, Y. I. Kim and Y. M. Kang, *J. Power Sources*, **230**, 138 (2013).
17. B. H. Song, M. O. Lai and L. Lu, *Electrochim. Acta* **80**, 187 (2012).